Fragmentation of carbon ions at 250 MeV/nucleon

J. M. Kidd
Naval Research Laboratory, Washington, D.C. 20375

P. J. Lindstrom
Lawrence Berkeley Laboratory, Berkeley, California 94720

H. J. Crawford
University of California, Berkeley, California 94720

G. Woods
Naval Research Laboratory, Orlando, Florida 32856
(Received 8 May 1987)

The single particle inclusive reactions $^{12}C + {}^{12}C \rightarrow x +$ anything ($3 \leq Z \leq 6$) have been studied at 250 MeV/nucleon at nine production angles from 0° to 4°. Production cross sections for most isotopes ($Z > 2$) were determined. The longitudinal and transverse momentum distributions were constructed. The results at this energy are compared to the data at other energies and to the model of Friedman. It appears that, after the Coulomb effects are separated, there is very little energy dependence in the fragmentation process.

INTRODUCTION

The study of projectile fragmentation began in 1948 (Ref. 1) when heavy nuclei were discovered in the cosmic radiation. After two decades, fragmentation of nuclei from the entire periodic table was surprisingly well understood despite formidable experimental difficulties.[2,3] The acceleration of heavy ions at the Princeton Particle Accelerator to energies near 0.5 GeV/nucleon and at the Bevatron at Lawrence Berkeley Laboratory to energies near 2 GeV/nucleon in 1971 allowed projectile fragmentation to be studied in a quantitative and straightforward way. Early measurements were made by Lindstrom *et al.*[4] and Greiner *et al.*[5] of the fragmentation of carbon ions at 1.05 GeV/nucleon and carbon and oxygen ions at 2.1 GeV/nucleon. These experiments showed that (1) the fragmentation cross sections factor,[6,7] (2) the energy transfers are very small, (3) the fragments are emitted isotropically in the projectile rest system, and (4) the widths of the momentum distributions of the fragments have a roughly parabolic dependence on the fragment mass. The hypothesis of limiting fragmentation is a very good approximation at these energies.

The present experiment was designed to study fragmentation at an energy at which limiting fragmentation may begin to break down. We studied the single-particle inclusive reactions of ^{12}C at 250 MeV/nucleon on a carbon target:

$$^{12}C + \text{target} \rightarrow X + \text{anything} , \quad (1)$$

where X was any ($Z > 2$) final-state fragment within the acceptance of the detector. This experiment was designed specifically to detect any differences in fragmentation from those at higher energies. These potential deviations include the following questions. (i) Are the cross sections energy dependent? (ii) Are the momentum distributions Gaussian, and are they independent of energy? (iii) What are the widths of the momentum distribution, and what is the fragment mass dependence of the widths? Are the widths of the transverse and longitudinal distribution the same? (iv) Can the descriptions of projectile fragmentation from 20 MeV/nucleon to 2.1 GeV/nucleon be unified, as has been suggested?[8,9]

The energy dependence of the production cross sections is determined by comparing them to the 1.05 and 2.1 GeV/nucleon carbon data and to the predictions of Friedman.[10] The longitudinal and transverse momentum distribution widths are compared to previous data,[5,11,12] and the mass dependence of the widths is compared to the models of Goldhaber[13] and Friedman.

EXPERIMENTAL SETUP

Carbon-12 ions were extracted and delivered to beam line 40 with an energy of 246 MeV/nucleon at the detector face with target out. The maximum intensity was 3×10^6 ions/spill. The experimental setup is shown in Fig. 1. The beam was incident on a carbon target which was 1.15 g/cm^2 thick and located 6.60 m upstream of the detector. The detector is shown at the downstream end of the vacuum tank. Data were taken at nine rail positions, each separated by approximately 0.5°. The largest rail position corresponded to 4.0°.

The isotope detector was designed as a Cherenkov-CsI telescope with beam-defining scintillation counters and drift chambers. The detector is shown in Fig. 2 and the dimensions of those elements used in this analysis are shown in Table I. High-density crystals (CsI and the Cherenkov radiator) with a small amount of scintillator

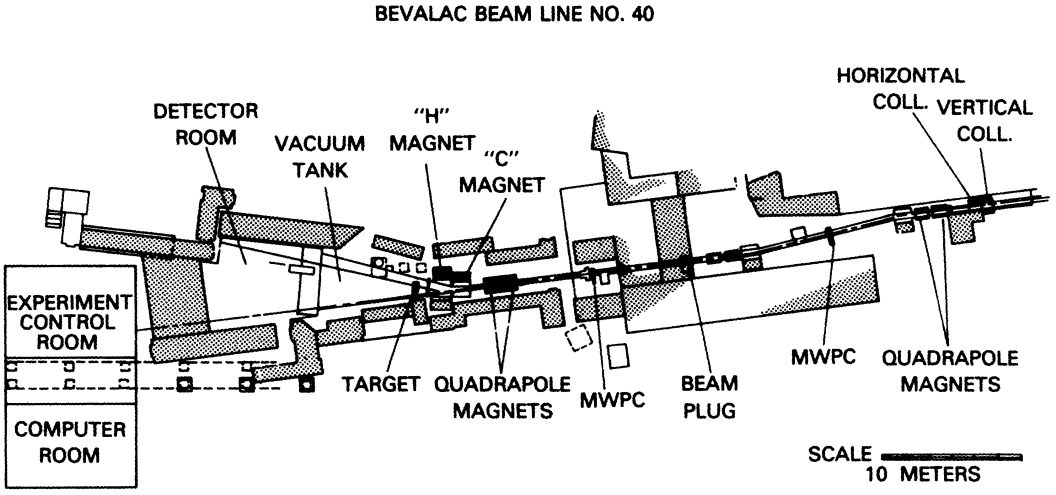

FIG. 1. Bevalac beam line 40.

helped to minimize interactions of the fragments in the detector.

The charge was determined directly from the $S1$ signal. The detector allowed two mass determinations (Cherenkov $\times E$ and $\Delta E \times E$) for each fragment and was able to resolve isotopes for $Z > 2$. The drift chamber allowed momentum quantities to be constructed and was used in the calculations of the acceptance of the detector for each isotope.

The detector was designed to study the $Z < 3$ fragments with the aid of the PA and PB counters (Fig. 2). This proved impossible because the Cherenkov counter had low photoelectron statistics for these charges, the PA resolution was worse than expected, and the PB counter

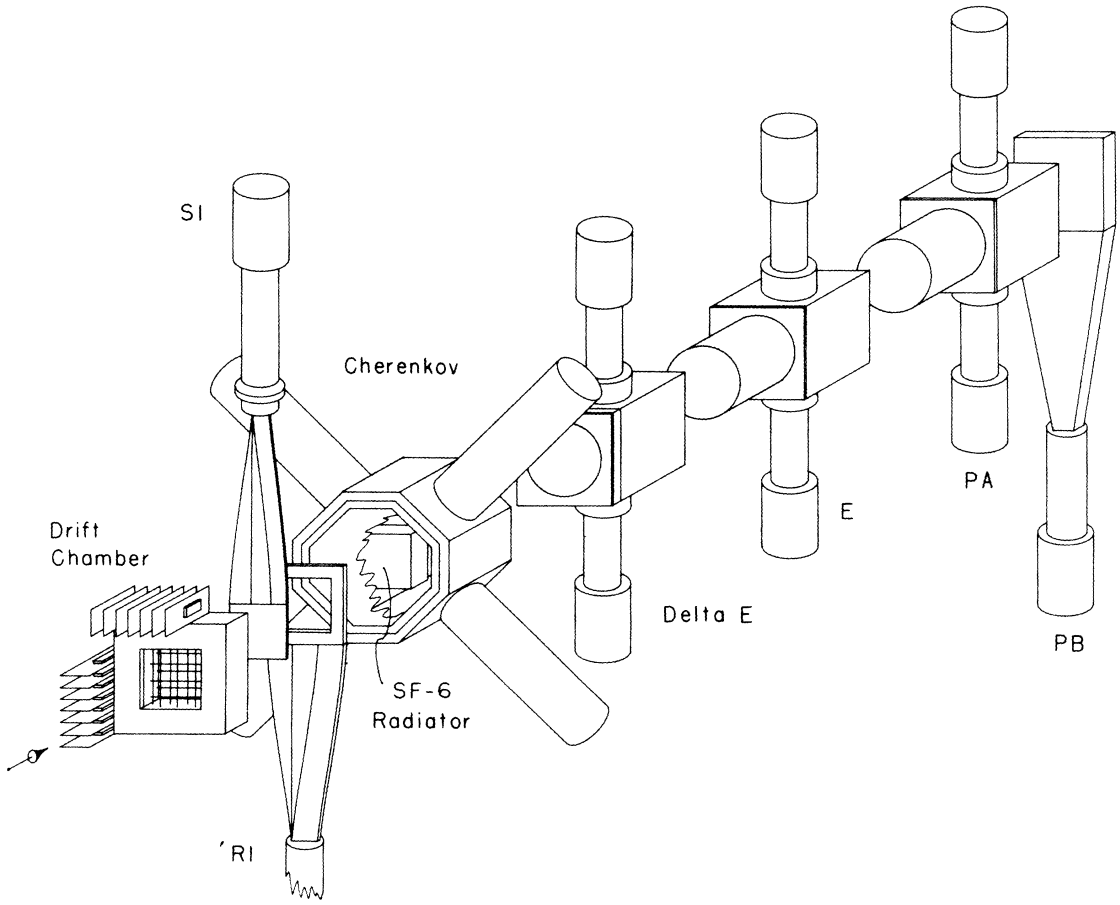

FIG. 2. Isometric projection of the detector.

TABLE I. The detector.

Element	Size and material (cm)	Density (g/cm^3)	Resolution (246 MeV/nucleon ^{12}C beam) (%)
$S1$	$6.35\times6.35\times0.635$ Pilot B	1.02	4.3
Cherenkov	$6.35\times6.35\times2.22$ SF-6 glass	5.18	7.9
ΔE	7.62 diam$\times$0.95 CsI	4.51	2.3
E	7.62 diam$\times$7.62 CsI	4.51	1.9

had an intermittent failure. Therefore, the results presented here are for fragments with $Z>2$.

The beam was monitored by a system which consisted of a particle counter, a current mode counter, and three counters which formed a secondary emission monitor (SEM). These counters were calibrated at the beginning of each run by increasing the beam intensity slowly and off line by performing a least-squares fit of all counters to the particle counter. The rms deviation among the five combinations of SEM counters was 1.2% for the runs below 2°, and 1.5% for the remainder.

The fast logic is shown in Fig. 3. An event trigger was defined as signals in the $S1$ and $S1'$ ($S1'$ was 1.6-mm-thick scintillator behind $S1$ not shown in Fig. 1), no pathological beam behavior ($tr2$), and computer not busy. The signals which were pulse heights analyzed were from the $S1$, Cherenkov, ΔE, and E counters. The Bevatron timing signals were used at the beginning and the end of each spill to enable and disable data taking. The Camac was read for each trigger, and each data file was written to tape. This data set was 12 files of 26 K 34-word events for target in and 11 similar files for target out.

ANALYSIS

The first step in the analysis of an event was the determination of the charge of the fragment directly from the $S1$ signal. Figure 4 shows the raw $S1$ spectrum for $Z>2$. Note that there is very little overlap, and any misassigned charges were corrected later by the minimization routine.

Next, two particle-identifier-type masses were determined: $\Delta E\times E$ and Cherenkov $\times E$ masses. The $\Delta E\times E$ mass is

$$M_{\Delta E\times E}=\frac{k}{Z^2}[(\epsilon+\Delta\epsilon)^{\alpha}-\epsilon^{\alpha}]^{1/\alpha-1}\,, \tag{2}$$

where $\Delta\epsilon$ and ϵ are the energy losses in the ΔE and E counters and are functions of the pulse heights from the

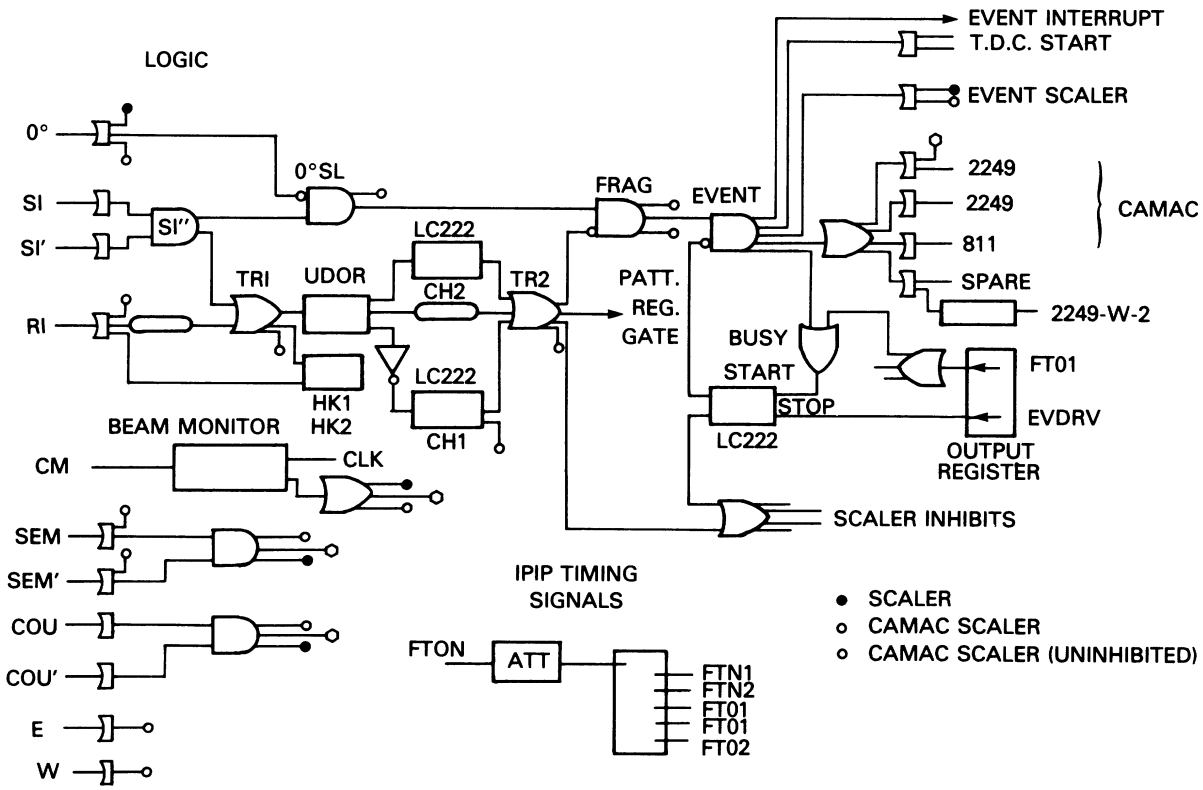

FIG. 3. Fast logic and beam monitors.

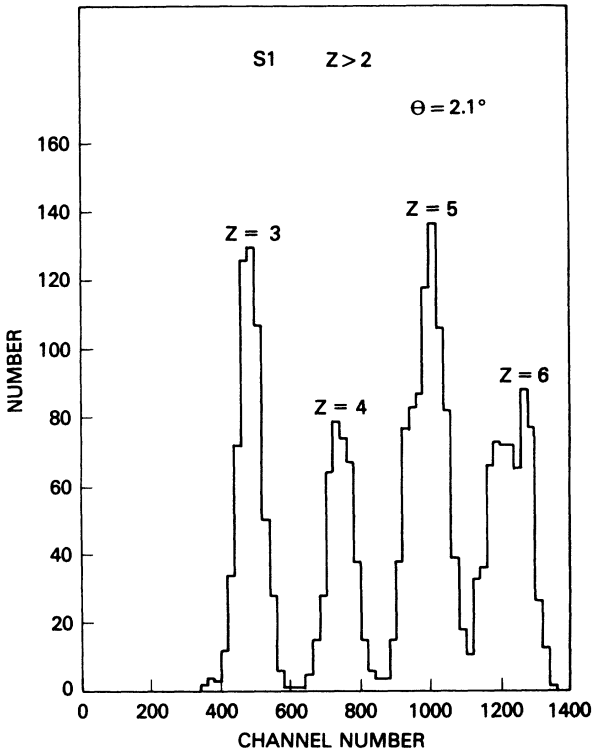

FIG. 4. $S1$ spectrum for $Z>2$ at a production angle of 2.1°.

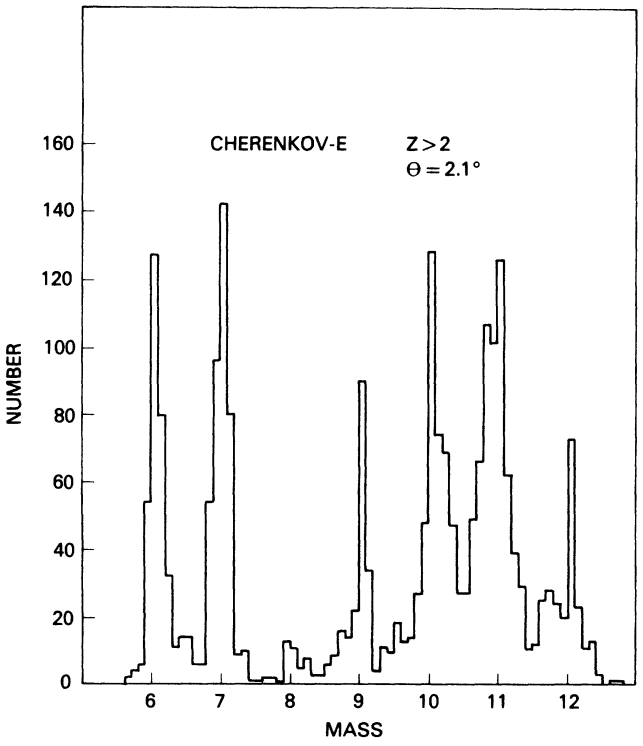

FIG. 5. Cherenkov-E mass determinator for $Z>2$ at a production angle of 2.1°.

ΔE and E signals. The exponent α is 1.68 with a very weak charge dependence.

The second mass assignment used the pulse heights from the Chernekov and E counters. For a thick Cherenkov radiator, the observed signal was an integral over the radiator ($\propto Z^2$) times the effective range ($\propto A/Z^2$) which yielded a signal proportional to the mass:

$$S_c = k\int Mf(B)F(B)dB = MG(B) \tag{3}$$

$$\propto MR^{\delta}\,, \tag{4}$$

where R is the range and δ is an exponent.

The range is related to the stopping signal (E counter) by:

$$R \propto M^{-0.69}S_E\,. \tag{5}$$

Then we have

$$S_c/M \propto (M^{-0.69})^{\delta}S_E^{\delta} \quad \text{or} \quad M^{\lambda} \propto S_E^{\delta}/S_c\,. \tag{6}$$

The two exponents λ and δ were found for each isotope. These (first-approximation) mass determinations are shown in Figs. 5 and 6. Note that the resolution of the Cherenkov $\times E$ is better than the $\Delta E \times E$ for all charges, because for $Z>2$, the Cherenkov counter has considerably better resolution than the ΔE counter.

Finally, a four term χ^2 ($S1$, Cherenkov, ΔE, and E) was constructed, and this was minimized with respect to charge, mass, and energy. The calculated response of the detector was compared to scatter plots of the data until they agreed at the 2% level. A similar approach has been used to determine the exponents for the mass identifiers.

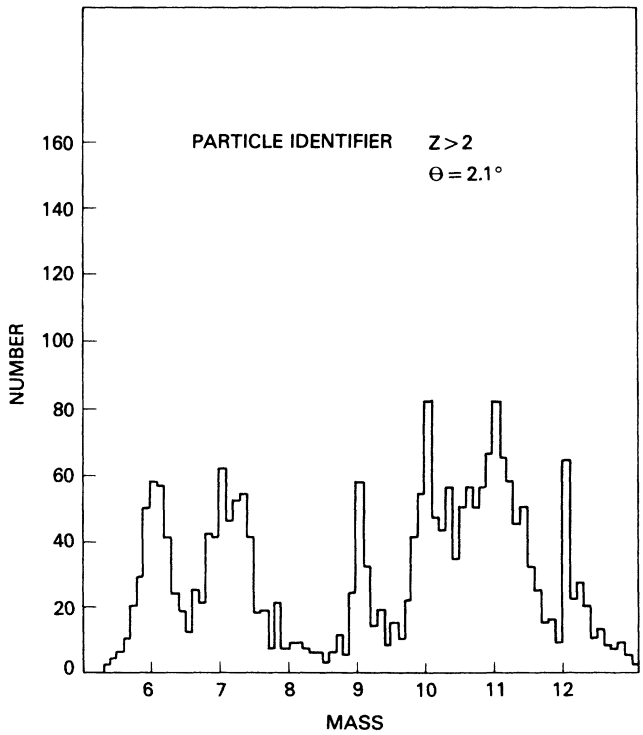

FIG. 6. Particle identifier mass determinator for $Z>2$ at a production angle of 2.1°.

ERRORS

Typically, the largest contribution to the errors on the cross sections was the statistical uncertainty of the observed number of fragments. The corrections made in the calculation of the cross sections are well known, and only occasionally did their uncertainties contribute appreciably to the final errors. The uncertainty in the scaler data used to normalize each angular position was 1.5% and contributed negligibly. The target-out files were typically a few percent ($<7\%$) of the target-in files. Table II shows for each isotope the rms statistical uncertainties from all rail positions.

The drift-chamber efficiency was less than unity, varying from 0.55 at $Z=3$ to 0.25 at $Z=6$. The cross sections, therefore, were determined using the good χ^2 events with no cut on the drift chamber. In order to determine whether there was any contamination by multiple-particle events, the number of good χ^2 was compared to the number of good χ^2 and good drift chamber (good x and y coordinates and single track) divided by the mean-drift-chamber efficiency for that charge. The difference between these numbers for each isotope was a measure of the systematic uncertainty. The third column in Table II shows the rms total systematic uncertainties, measured in this manner.

MOMENTUM DISTRIBUTIONS AND WIDTHS

The momentum quantities were constructed for those triggers with good χ^2 and good drift chamber. The longitudinal widths were determined by fitting the projectile rest system distribution (P^*) for each isotope to a Gaussian function. The fit also determined the mean of each distribution. This was repeated for all rail positions. Table III shows the results of these fits. The errors are from a nonlinear maximum-likelihood analysis of each distribution. The rms widths, averaged over all rail positions for each isotope, are shown in Table IV. These results will be discussed later.

The widths of the transverse momentum distributions were wider than anticipated when the data were taken. We planned to determine the widths by analyzing the

TABLE II. Error quantities.

Isotope	rms statistical (%)	rms systematic (%)
^{6}Li	9.46	6.26
^{7}Li	11.71	9.17
^{8}Li	43.07	30.61
^{7}Be	10.41	10.95
^{9}Be	13.54	19.47
^{10}Be	18.12	14.62
^{8}B	23.31	40.17
^{10}B	6.39	7.48
^{11}B	5.57	8.47
^{12}B	49.27	23.29
^{10}C	17.99	44.21
^{11}C	5.82	10.49

TABLE III. Parallel momentum distribution widths and means (projectile rest system). Results of fits by isotope and production angle.

Production angle	0.4	0.8	1.3	1.7	2.1	2.6	3.0	3.9
				Widths (MeV/c)				
^{6}Li		100.70± 7.4	88.10± 7.9	88.40± 5.6	101.90± 7.1	95.90± 6.3	102.00± 7.1	115.20± 6.8
^{7}Li		75.80± 5.1	80.30± 8.3	109.00± 8.4	108.30± 7.7	108.00± 7.4	107.80± 6.7	110.20± 5.6
^{7}Be	106.40±45.8	122.70± 9.0	125.90±10.6	119.60±10.1	96.40± 8.9	112.10± 9.3	114.30±15.7	95.90± 9.9
^{9}Be		80.90± 9.0	116.60±11.5	129.20±15.5	87.40±13.5	109.10±11.3	69.90±15.5	86.60±15.1
^{10}Be		117.10±19.8	113.90±12.3	108.80±25.3	81.40±11.3	119.50±17.6	115.40±23.6	110.00±20.0
^{10}B	141.80±36.0	107.90±11.0	152.40±19.4	106.40±13.5	110.20±12.8	97.20±10.1	105.60±14.8	94.10± 8.0
^{11}B	99.10±18.1	93.60± 7.8	98.60± 9.5	92.20± 9.7	102.70±11.0	106.90±12.1	89.10±13.7	101.40±12.2
^{11}C	62.20± 5.1	76.30± 7.5	72.30± 8.3	88.10± 7.0	90.90±10.0	87.20± 7.4	64.10±33.7	96.20± 9.8
				Means (MeV/c)				
^{6}Li		−108.60±10.1	−125.00± 9.5	−106.80± 9.7	−110.70±11.2	−135.00±10.3	−123.90±10.5	−142.90±28.7
^{7}Li		−177.70±10.7	−171.70±10.6	−146.50±16.3	−137.90±15.7	−180.40±15.6	−164.70±14.1	−168.30±11.7
^{7}Be	15.00±44.0	−72.60±15.2	−69.50±15.9	−86.00±14.6	−85.00±12.1	−89.20±13.3	−96.50±13.4	−82.10±10.1
^{9}Be		−86.90±12.3	−83.40±17.8	−86.70±19.4	−101.40±12.1	−115.90±19.9	−164.20±16.5	−130.20±16.7
^{10}Be		−156.10±23.4	−87.00±20.5	−113.10±22.7	−187.00±17.0	−141.60±22.2	−152.30±25.2	−120.90±20.0
^{10}B	−9.90±45.4	−66.40±12.6	−14.80±19.0	−72.90±15.2	−92.00±16.1	−99.90±13.1	−102.00±14.9	−150.00±10.2
^{11}B	−22.00±23.4	−45.40±13.7	−59.40±14.2	−77.80±13.4	−120.00±15.6	−120.00±15.6	−109.10±14.1	−146.00±13.2
^{11}C	48.60±10.1	−8.90±9.6	−16.60±10.4	−22.30±12.9	−26.50±15.2	−56.70±15.2	−68.30±13.4	−86.80±20.5

TABLE IV. rms parallel momentum distribution widths and rms means (projectile rest system).

	(MeV/c)			
	Width	Error	Mean	Error
^{6}Li	98.9	6.9	−121.8	10.0
^{7}Li	99.9	7.1	−163.9	13.7
^{7}Be	111.7	19.0	−70.7	20.1
^{9}Be	97.1	13.3	−109.8	16.6
^{10}Be	109.4	19.2	−136.9	21.7
^{10}B	114.4	17.8	−75.0	21.1
^{11}B	97.9	12.1	−87.6	15.6
^{11}C	79.7	14.1	−29.7	13.8

momentum quantities for each of the nine rail positions and summing each file after normalizing by the acceptance of the detector. These distributions would determine the widths for each isotope. The transverse momentum distributions were so wide that 4° was not sufficiently large to construct the complete transverse distributions directly, certainly not for the small masses.

We therefore formed the quantity

$$\ln\left[\frac{1}{p_\perp}\frac{\partial\sigma}{\partial p_\perp}\right]$$

for each isotope and each rail position. This was plotted versus the square of the transverse momentum. A plot for each isotope is shown in Figs. 7 and 8. The errors shown include the statistical and systematic contributions. Note that in all cases, a least-squares fit was made for each isotope to the five points with the largest $P_\perp$. These results are shown in Table V.

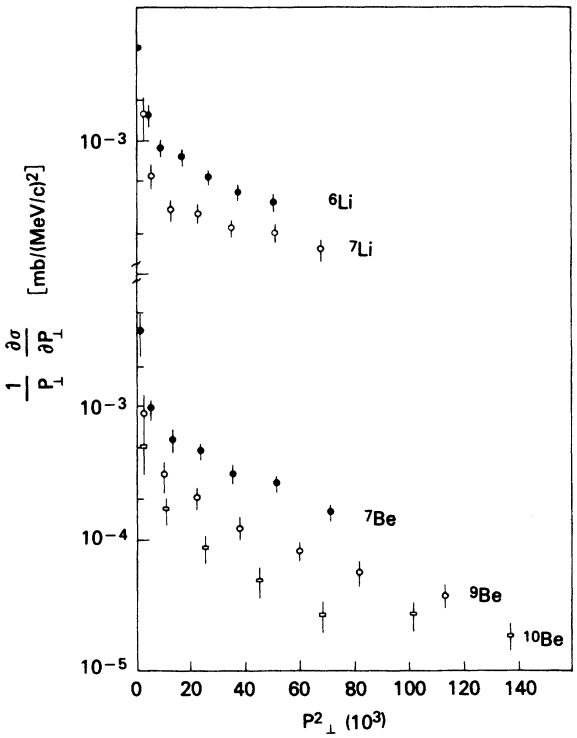

FIG. 7. Transverse momentum distributions for lithium and beryllium isotopes.

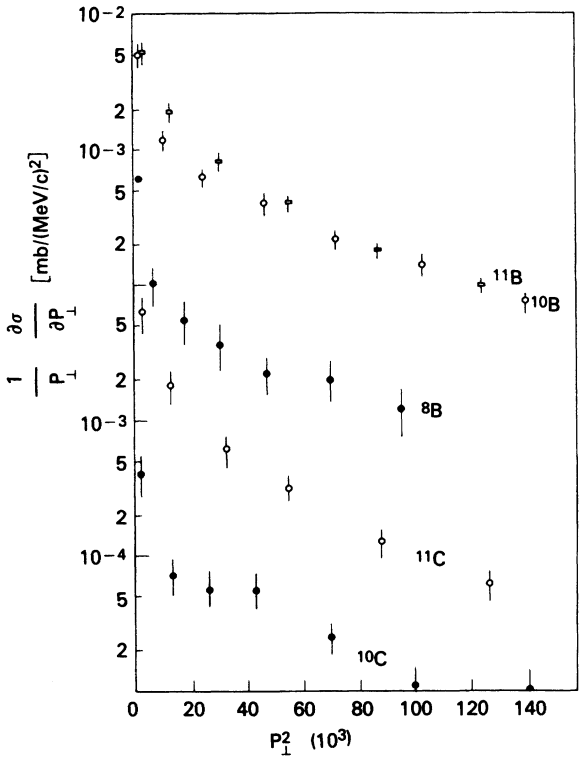

FIG. 8. Transverse momentum distributions for boron and carbon isotopes.

CROSS SECTIONS

The acceptance of the detector was computed for each isotope and rail position (integrating over the beam profile and taking into account the rigidity gradient for each isotope). The target-out runs were treated in a similar fashion but contributed negligibly. In Figs. 9 and 10,

TABLE V. Transverse momentum distribution widths.

	(MeV/c)
^{6}Li	146.62±12.42
^{7}Li	200.85±11.08
^{8}Li	172.08±25.18
^{7}Be	153.26± 5.73
^{9}Be	167.12±18.06
^{10}Be	201.54±35.29
^{11}Be	118.84±20.13
^{8}B	165.09±15.03
^{10}B	166.02± 6.23
^{11}B	153.65± 7.23
^{12}B	145.13±20.86
^{10}C	176.68±37.14
^{11}C	152.72±11.87

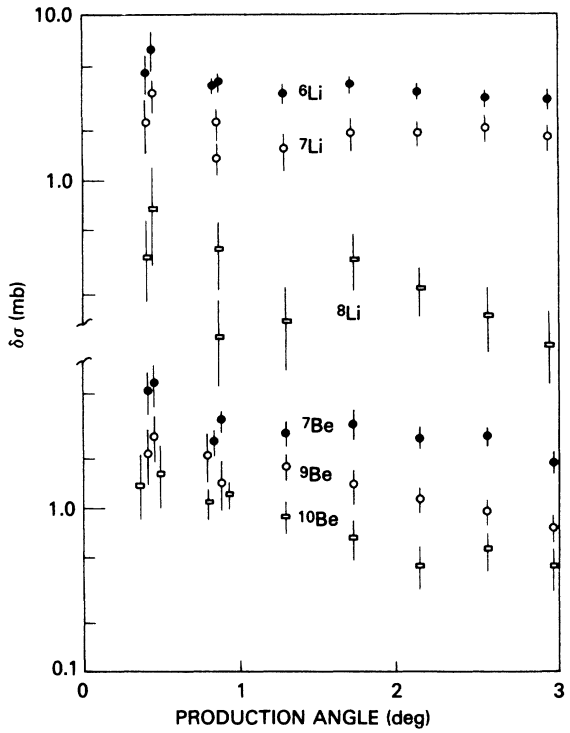

FIG. 9. Differential cross sections vs production angle for lithium and beryllium isotopes.

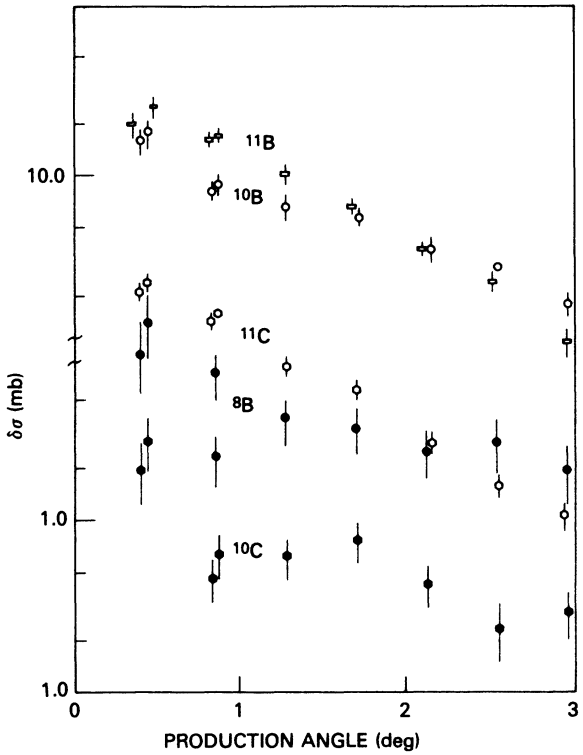

FIG. 10. Differential cross sections vs production angle for boron and carbon isotopes.

the cross-section contribution from each isotope is shown versus detector position. The errors include statistical and systematic contributions.

There is a correction which must be applied to the small-mass isotopes with large transverse widths. This is simply because all of the cross section could not be measured within 4°. The correction is 15% for ^{6}Li, 22% for ^{7}Li, 11% for ^{8}Li, and 11% for ^{7}Be and is a maximum of a few percent for the larger masses.

The cross sections from this experiment are shown in the first column of Table VI. The errors include statistical and systematic contributions. ^{8}B and ^{12}B are quoted as upper limits only, because without a drift chamber with unit efficiency, it is not possible to separate these isotopes from ^{10}B and ^{11}B reliably.

DISCUSSION OF RESULTS

Cross sections

The cross sections from this experiment are listed in Table VI together with those measured at 1.05 and 2.1

TABLE VI. Carbon-data cross sections.

	(mb)			
	250 MeV/nucleon	1.05 GeV/nucleon[a]	2.1 GeV/nucleon[a]	Friedman[b]
^{6}Li	26.35±2.1	27.10±2.20	30.00±2.40	19.6
^{7}Li	> 17.19±1.3	21.50±1.10	21.50±1.10	14.2
^{8}Li	> 1.33±0.34	2.40±0.18	2.19±0.15	2.5
^{7}Be	22.64±1.49	18.60±0.90	18.40±0.90	13.3
^{9}Be	10.44±0.85	10.70±0.50	10.60±0.50	13.8
^{10}Be	5.88±9.70	5.30±0.30	5.81±0.29	7.1
^{11}Be	0.36±0.26			
^{8}B	< 3.21±0.59	1.43±0.10	1.72±0.13	2.1
^{10}B	47.50±2.42	27.90±2.20	35.10±3.40	22.1
^{11}B	65.61±2.55	48.60±2.40	53.80±2.70	42.2
^{12}B	< 0.49±0.67	0.10±0.01	0.10±0.01	
^{10}C	5.33±0.81	4.44±0.24	4.11±0.22	6.1
^{11}C	55.97±4.06	44.70±2.80	46.50±2.30	41.3

[a]Reference 4.
[b]Reference 10.

GeV/nucleon and those predicted by Friedman. The ratio of the cross sections from this experiment to those at 1.05 GeV/nucleon is shown in Fig. 11. It is apparent that the major departure from the high-energy data appears in the single- and double-nucleon cross sections ^{11}C, ^{11}B, and ^{10}B. Surprisingly, ^{10}B shows the largest departure from the 1.05 GeV/nucleon data. There is a correction to the ^{10}B cross section from beam particles which interacted between the target and the detector and produced fragments with the beam charge to mass ratio, in particular ^{10}B. This correction is estimated to be approximately 2% (and has been applied), so that even with the correction, ^{10}B is large. As already mentioned, ^{7}Li could not be measured accurately, so the quoted value may be slightly low. The energy dependence in this data is surprisingly small.

In the last column in Table VI are the predictions from the model of Friedman for ^{12}C projectiles. In this paper, Friedman quotes relative isotopic yields. We have taken the liberty of multiplying these yields by the target factor in order to compare them directly with the measurements, but one should keep in mind that these predictions are primary yields which may be modified by subsequent decay of the fragments. With the exception of the single- and double-nucleon cross sections and possibly ^{8}Li, the agreement is not unreasonable. Friedman's assumption (that for energies larger than the Coulomb barriers involved in the entrance and exit channels, certain aspects of the fragmentation process will be independent of target and projectile energy) seems to be correct down to the energy of this experiment.

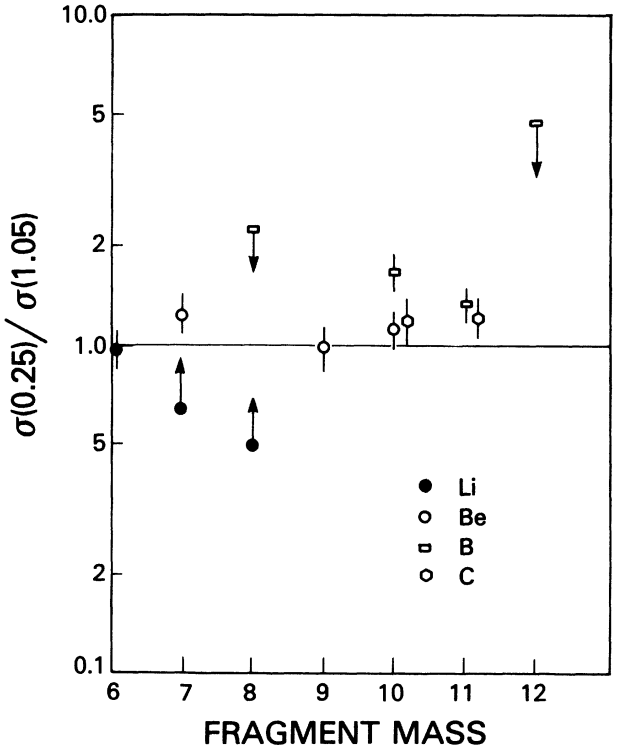

FIG. 11. Ratios of cross sections from this experiment to those at 1.05 GeV/nucleon.

MOMENTUM DISTRIBUTIONS

The longitudinal and transverse momentum distribution widths have been predicted by several independent theories to have a parabolic dependence:[10,13–16]

$$\sigma_{\parallel}=\sigma_0\left[\frac{F(B-F)}{B-1}\right]^{1/2}. \tag{7}$$

This dependence allows the Fermi momentum and the average excitation energy to be derived.[5] Recently, Friedman developed an elegant model for the parallel momentum distribution.[10] This model relates the widths to the separation energy and an absorptive cutoff radius. The parabolic mass dependence arises in this model because the separation energy is roughly proportional to the mass number of the fragment times the separation energy of a single nucleon. The agreement with the high-energy carbon data is excellent. In this model the widths of the paralleled momentum distributions have the form:

$$\sigma_{\parallel}^2=\frac{\mu}{2x_0}\left[\frac{1+\frac{1}{2}y}{\sqrt{(1+y)}}+\frac{1}{\mu x_0}\right], \tag{8}$$

where μ is given by:

$$\mu=\sqrt{(2m_r E_s)}, \tag{9}$$

and m_r is the reduced mass, and E_s is the separation energy. The expression for y is

$$y=\frac{Z_1 Z_2 e^2}{x_0 E_s} \tag{10}$$

and x_0 is 1.2 fm. The first term in brackets essentially takes into account the effect of the Coulomb potential on the tail of the bound state wave function.

The rms longitudinal momentum widths are shown in Table VII. These are compared directly with the carbon data at 1.05 and 2.1 GeV/nucleon and Friedman's predictions. We list only those isotopes which we were able to measure in this experiment. The widths of the ^{6}Li and ^{7}Li measured here are probably too narrow. This is because the distributions averaged were preferentially the low-transfer-momentum bites. These widths are quoted as lower limits. The widths are systematically narrower than those of the high-energy data, approximately 1.5σ below those at 1.05 GeV/nucleon. We do not feel that this is a real effect. The longitudinal widths measured at 87, 90, 120, and 213 MeV/nucleon[11,12,17] all agree quite well with the high-energy data as expected, because Coulomb effects should not change the longitudinal widths.

Because the widths are expected to be independent of target, projectile, and possibly energy, data with other targets at other energies and projectiles are listed in Table VIII. Here, for simplicity, we list the σ_0 fitted to each data set. The carbon data show a very weak energy dependence at the one-sigma level, but there seems to be a larger projectile mass dependence.

TABLE VII. rms parallel momentum distribution widths (projectile rest system) carbon data (MeV/c).

	This experiment $\sigma_0=67\pm3.5$	1.05 GeV/nucleon $\sigma_0=70.5\pm2.5$	2.1 GeV/nucleon $\sigma_0=73.5\pm2.0$	Friedman
^{6}Li	98.9±7.0	122.0±10.0	127.0±7.0	149.0
^{7}Li	99.9±7.0	142.0± 7.0	144.0±2.0	142.0
^{7}Be	111.7±19.0	140.0± 6.0	145.0±2.0	143.0
^{9}Be	97.1±13.0	131.0± 9.0	133.0±3.0	128.0
^{10}Be	109.4±19.0	125.0±11.0	129.0±4.0	124.0
^{10}B	114.4±18.0	135.0± 9.0	134.0±3.0	120.0
^{11}B	97.9±12.0	102.0±11.0	106.0±4.0	102.0
^{11}C	79.7±14.0	105.0±10.0	103.0±4.0	103.0

Greiner *et al.*[5] found an approximately linear relationship between the average momentum mean and the widths, except for charge exchange and charge exchange plus one nucleon. The average momentum was slightly negative (velocity less than beam) with respect to the projectile with a mean of 30 MeV/c. Fragments resulting from charge exchange had larger means of 100 MeV/c. The means from this experiment are shown in Table III. The uncertainties in the means are large because of the drift-chamber efficiency. Nevertheless, we argue that the same amount of energy is transferred to the fragment (similar $\sigma_{\parallel}$). This will result in a larger negative mean because there is less energy in the P.R.S. The average mean in this data is -99.5 ± 48.1 MeV/c. The uncertainties in these data are too large to confirm the linear relation between means and widths, but they do not preclude it.

The transverse momentum widths are shown in Table V. At high energy, the measurements of Greiner *et al.*[5] showed that the widths of the transverse momentum distributions were equal to those of the longitudinal ones within 10%. At 250 MeV/nucleon, one might expect Coulomb scattering to contribute to the widths. In order to investigate this qualitatively, we formed:

$$\sigma_{\text{Coulomb}}(Z,A)=P_{\text{total}}(Z,A)\sin\left[\frac{Z_1Z_2e^2}{Eb}\right], \qquad (11)$$

where E is the total kinetic energy. The argument of the sine is the angle through which the fragment is scattered by the target and projectile residue, and b is the impact parameter. The two contributions should add in quadrature so that one can subtract the Coulomb contribution.

TABLE VIII. σ_0 from other experiments.

Energy (GeV/nucleon)	Projectile	Target	σ_0 (MeV/c)
0.25	Carbon	Carbon	67.5±3.5
1.05	Carbon	Carbon	70.5±2.5 (5)
2.1	Carbon	Carbon	73.5±2.0 (5)
0.52	Nitrogen	Hydrogen	73.0±5.0 (18)
0.087	Carbon	Carbon	109.0 at 4° (12)
			65.0 at 8°
0.092	Oxygen	Gold	80.0 (11)
0.092	Oxygen	Aluminum	86.0 (11)
2.1	Oxygen	Carbon	85.5±1.5 (5)
0.21	Argon	Carbon	94.0±5.0 (17)

We do not know the impact parameters, but with reasonable assumptions about them, we find that the widths without the Coulomb contribution agree quite well with the 1.05 and 2.1 GeV/nucleon data. The results and the assumed impact parameters are shown in Table IX. Note that the lighter fragments have smaller impact parameters (larger overlap and larger residue), and the heavier fragments have larger impact parameters. This is consistent with the simplest mechanism of fragmentation in which the residue interacts with the target. We have not done a fit because the data are not sufficiently accurate to warrant one.

This is certainly not conclusive, but this type of Coulomb scattering has been seen at lower energy. At 87, 90, and 120 meV/nucleon[11,12] the measurements showed that the transverse widths were approximately 200 MeV/c. Van Bibber *et al.* interpreted this dispersion as orbital deflection of the ^{16}O projectile by the combined Coulomb field of the target together with the usual dispersion due to the Fermi motion. No broadening was seen in the transverse momentum widths from the nitrogen data at 0.52 GeV/nucleon,[18–32] but this could well be because the target was hydrogen.

CONCLUSIONS

The energy dependence of the cross sections seems to be confined to the one- and two-nucleon removal cross sections. With the exception of ^{11}C, ^{11}B, and ^{10}B, there appears to be very little difference from the high-energy data. However Buenerd *et al.*[8] pointed out some time ago the remarkable similarity of cross sections at 20 MeV/nucleon and 2.1 GeV/nucleon. As mentioned earlier, Friedman's arguments about the energy independence of the fragmentation process seem to be very good at this energy.

The longitudinal momentum widths measured here are similar to those at other energies but slightly narrower. All other experiments measure widths which are very close to the high-energy data. We conclude that the longitudinal momentum widths at this energy are similar to those measured from 87 MeV/nucleon to 2.1 GeV/nucleon.

Greiner *et al.*[5] found that all centers were negative with respect to the projectile. The uncertainties in this data are large, but we find larger negative centers as one would expect at this energy. These data are not accurate

TABLE IX. Carbon transverse momentum distribution widths with Coulomb correction.

	b (fm)	This experiment	(MeV/c) 1.05 GeV/nucleon	2.1 GeV/nucleon
^{6}Li	1.00	125.0±15.0	122.0±10.0	127.0± 7.0
^{7}Li	1.07	187.0±14.0	142.0± 6.0	144.0± 2.0
^{7}Be	1.07	132.0± 7.0	140.0± 6.0	145.0± 2.0
^{9}Be	1.22	145.0±21.0	131.0± 9.0	133.0± 3.0
^{10}Be	1.30	156.0±38.0	125.0±11.0	129.0± 4.0
^{8}B	1.15	123.0±16.0	139.0±12.0	151.0±16.0
^{10}B	1.30	134.0± 8.0	135.0± 9.0	134.0± 3.0
^{11}B	1.35	121.0± 8.0	102.0±11.0	106.0± 4.0
^{11}C	1.35	104.0±11.0	105.0±10.0	103.0± 4.0

enough to check the linear dependence of the centers and the widths.

The transverse momentum widths measured here are large. We feel that there is a Coulomb contribution at this energy which, when subtracted roughly, yields transverse widths which are consistent with the high-energy data. More accurate data are needed to separate Coulomb effects accurately at this energy.

The nuclear fragmentation at 250 MeV/nucleon shows very little energy dependence (except for the single- and double-nucleon cross sections) when compared to the 1.05 and 2.1 GeV/nucleon data. The nuclear fragmentation mechanism appears to be virtually identical with that at high energy. However, the energy here is low enough that there is an additional contribution to the transverse widths from Coulomb scattering of the fragment.

It was first pointed out by Greiner *et al.*[5] that there was strong and recurring evidence of nuclear structure effects in their data. This is true in this experiment. Nevertheless, we conclude that so long as one can separate Coulomb effects, the fragmentation process is surprisingly energy independent from 20 MeV/nucleon to 2.1 GeV/nucleon—an economic and elegant conclusion.

ACKNOWLEDGMENTS

We should like to thank a number of people who helped in the various stages of this experiment. We thank B. Stiller and N. Seeman for help in the design, construction, and calibration of the detector. We thank L. Beahm, K. DeAngeles, G. Mueller, and C. MacParland for help in writing the data acquisition and real-time operating systems. We thank F. Beiser, M. Flores, D. Greiner, and T. J. M. Symons for help in staging and data taking. We thank the entire Bevatron staff, in particular, J. Alonzo, B. Everett, and H. Ellison. Finally, we thank J. B. Aviles, Jr., for his help throughout the analysis.

[1]P. Frier, E. J. Lofgren, E. P. Ney, and F. Oppenheimer, Phys. Rev. **74**, 1818 (1949); H. L. Bradt, *ibid.* **74**, 213 (1949).

[2]C. F. Powell, P. H. Fowler, and D. H. Perkins, *The Study of Elementary Particles by the Photographic Method* (Pergamon, New York, 1959).

[3]J. M. Kidd, in *High Energy Physics,* edited by E. H. S. Burhop (Academic, New York, 1967).

[4]P. J. Lindstrom, D. E. Greiner, H. H. Heckman, B. Cork, and F. S. Beiser, L. B. L. Report No. LBL3650, 1975 (unpublished).

[5]D. E. Greiner, P. J. Lindstrom, H. H. Heckman, B. Cork, and F. S. Beiser, Phys. Rev. Lett. **35**, 152 (1975).

[6]J. Coguon and R. Sartov, Phys. Rev. C **21**, 2342 (1980).

[7]D. L. Olson, B. L. Berman, D. E. Greiner, H. H. Heckman, P. J. Linstrom, and H. J. Crawford, Phys. Rev. C **28**, 1602 (1983).

[8]M. Buernard, C. K. Gelbke, B. G. Harvey. D. L. Hendrie, J. Mahoney, A. Memchaca-Rocha, C. Olmer, and D. K. Scott, Phys. Rev. Lett. **37**, 1191 (1976).

[9]J. Hufner, C. Sander, and G. Wolschin, Phys. Lett. **73B**, 289 (1978).

[10]William Friedman, Phys. Rev. C **27**, 569 (1983).

[11]K. Van Bibber, D. L. Hendrie, D. K. Scott, H. H. Weiman, L. S. Schroeder, J. V. Geaga, S. A. Ceissin, R. Treuhaft, Y. J. Groissord, J. O. Rasmussen, and C. Y. Wong, Phys. Rev. Lett. **43**, 840 (1979).

[12]J. Mougey, R. Ost, M. Buenerd, A. J. Cole, C. Guet, D. Lebrun, J. M. Loiseaux, P. Martin, E. Maurel, E. Monnand, H. Nifenecker, P. Perrin, J. Pinston, C. Ristori, P. deSaintignon, F. Schussler, L. Carlen, B. Jakobsson, A. Oskarsson, I. Otterlund, B. Schroder, H. A. Gustafsson, T. Johansson, H. Ryde, J. P. Bondorf, O. B. Nielsen, and G. Tibell, Phys. Lett. **105B**, 25 (1981).

[13]A. S. Goldhaber, Phys. Lett. **53B**, 306 (1974).

[14]W. A. Wenzel (unpublished).

[15]H. Feshbach and K. Huang, Phys. Lett. **47B**, 300 (1973).

[16]J. V. Lepore and R. J. Riddell, Jr., Lawrence Berkeley Laboratory Report No. 3086, 1974 (unpublished).

[17]Y. P. Viyogi, T. J. M. Symons, P. Doll, D. E. Greiner, H. H. Heckman, D. L. Hendrie, P. J. Lindstrom, J. Mahoney, D. K. Scott, K. Van Bibber, G. D. Westfall, H. Weiman, H. J. Crawford, C. MacParland, and C. K. Gelbke, Phys. Rev. Lett. **42**, 33 (1979).

[18]J. P. Wefel, J. M. Kidd, W. Schimmerling, and K. G. Vosburgh, Phys. Rev. C **19**, 1380 (1979).
[19]H. H. Heckman, D. Greiner, P. J. Lindstrom, and F. S. Bieser, Phys. Rev. Lett. **28**, 926 (1972).
[20]G. D. Westfall, Lance W. Wilson, P. J. Linstrom, H. J. Crawford, D. E. Greiner, and H. H. Heckman, Phys. Rev. C **19**, 1309 (1979).
[21]L. Anderson, W. Brockman, E. Moeller, S. Nagamiya, S. Nissen-Meyer, L. Schroeder, G. Shapiro, and H. Steiner, Phys. Rev. C **28**, 1224 (1983).
[22]H. H. Heckman and P. J. Lindstrom, Phys. Rev. Lett. **37**, 56 (1976).
[23]D. L. Olson, B. L. Berman, D. E. Greiner, H. H. Heckman, P. J. Lindstrom, G. D. Westfall, and H. J. Crawford, Phys. Rev. C **24**, 1529 (1981).
[24]C. Wong and K. Van Bibber, Phys. Rev. C **25**, 2990 (1982).
[25]J. P. Sullivan, J. A. Bistirlich, H. R. Bowman, R. Bossingham, T. Bottke, K. M. Crowe, K. A. Frankel, C. J. Martoff, J. Miller, D. L. Murphy, J. O. Rasmussen, W. A. Zajc, O. Hashimoto, M. Koike, J. Peter, W. Benenson, G. M. Crawley, E. Kashy, and J. A. Nolen, Jr., Phys. Rev. C **25**, 1499 (1982).
[26]G. Bertsch and Phillip J. Siemens, Phys. Lett. **126B**, 9 (1983).
[27]J. Nagamiya, J. Randrup, and T. J. M. Symons, Ann. Rev. Nucl. Part. Sci. **34**, 155 (1984).
[28]L. W. Townsend, J. W. Wilson, and J. W. Norbury, Can. J. Phys. **63**, 135 (1985).
[29]R. Babinet, Ann. Phys. (Paris) **11**, 113 (1986).
[30]J. Cugon, Ann. Phys. (Paris) **11**, 201 (1986).
[31]C. Gregore and B. Tamain, Ann. Phys. (Paris) **11**, 323 (1986).
[32]J. W. Wilson, L. W. Townsend, and F. F. Badavi, Nucl. Instrum. Methods **B18**, 225 (1987).

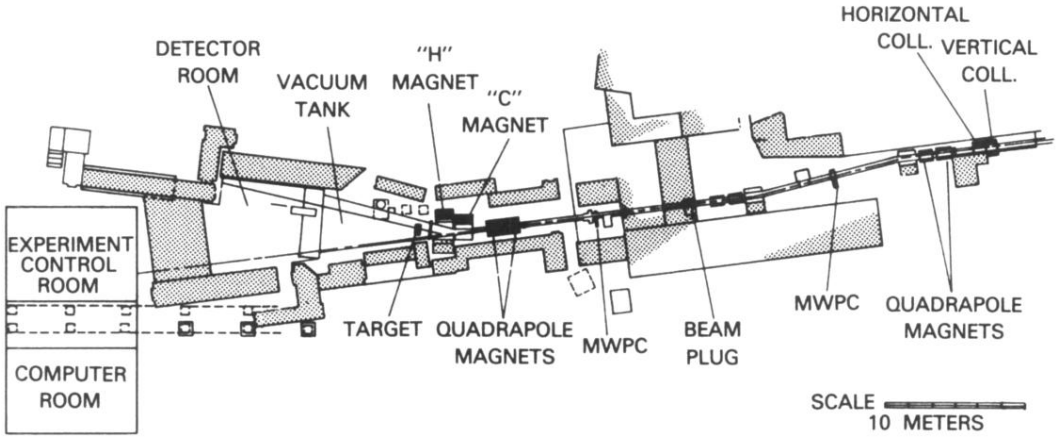

FIG. 1. Bevalac beam line 40.